Chemical Science

rsc.li/chemical-science

ROYAL SOCIETY
OF **CHEMISTRY**

EDGE ARTICLE
Yu Cao, Mingming Zhang *et al.*
Metallacycle-cored luminescent ionic liquid crystals with
trigonal symmetry

15 YEARS
ANNIVERSARY

Check for updates

Metallacycle-cored luminescent ionic liquid crystals with trigonal symmetry†

Long Chen,[ac] Yu Cao, [ID] *[a] Haohui Huo,[a] Shuai Lu,[b] Yali Hou,[a] Tianyi Tan,[a] Xiaopeng Li, [ID] [b] Feng Liu [ID] [a] and Mingming Zhang [ID] *[a]

Herein, we report the preparation of a series of metallacycle-cored liquid crystals with hexagonal and trigonal symmetries based on the self-assembly of tri(ethyl glycol) (TEG)-functionalized diplatinum(II) ligands and alkyl chain-appendant tetraphenylethylene (TPE) derivatives. Interestingly, with the increase of the density of the TEG units in the metallacycles, the phase separation between TEG and alkyl chains reduces the symmetry of the columnar phase from hexagonal *p6mm* to trigonal *p3m1*, which significantly enhances the aggregation of TPE units and thus increases the emission of the system, resulting in fluorescence quantum yield as high as 47.4% in the mesogenic phase. Moreover, the positive charges of the metallacycles endow these liquid crystals with good ionic conductivity at room temperature, making them potential candidates for optoelectronics.

Introduction

Macrocycles play a vital role in the development of supramolecular chemistry owing to their molecular recognition and complexation properties.[1–5] Furthermore, the self-assembly of macrocycles can generate favorable channels *via* molecular stacking, leading to the design of functional materials for the transportation of ions and molecules.[6–8] In particular, the formation of mesogenic phases endows the materials with good orientation and ordered nanostructures, making them useful materials for absorption, separation, sensing and transportation.[8–15] Therefore, various covalent macrocycles have been used as the cores to prepare macrocycle-cored liquid crystals to deliver different functions.[16–19] However, this strategy generally requires tedious chemical synthesis to decorate flexible chains onto the macrocycles to provide them sufficient mobility for suitable molecular stacking and liquid crystallinity.[20] In order to solve this problem, macrocycles formed by non-covalent interactions are developed,[21] with the aim to simplify the synthesis with their liquid crystalline properties well-retained.

Metal-coordination interactions have been widely applied for the construction of supramolecular coordination complexes

(SCCs)[22–28] with certain stability owing to their good directionality and moderate bond strength.[29–32] These SCCs, including metallacycles and metallacages, possess well-defined shapes, sizes and geometries, making them an ideal platform for further constructing ordered supramolecular assemblies with increased complexity *via* hierarchical self-assembly. Therefore, various interesting supramolecular structures, including supramolecular polymers, networks and gels, and liquid crystals have been prepared through SCC-based hierarchical self-assembly. Recently, we have reported a type of emissive rhomboidal metallacycle-cored liquid crystals, which exhibits a columnar phase and shows potential for the preparation of optoelectronic materials.[33] However, these liquid crystals only show moderate emission, and their conductivity has not been explored. For liquid crystal displays (LCDs), the mesogenic materials should be both highly emissive and sufficiently conductive to offer the device certain brightness, efficiency as well as electroluminescence.[34–37] Therefore, liquid crystals with high quantum yields and ion-conductivities are urgently needed for both devices and fundamental research.

Herein, we report four hexagonal metallacycles with varied densities of tri(ethylene glycol) (TEG) units (Scheme 1) which show both emission and ionic conductivity in the mesogenic phase. All these metallacycles show a hexagonal columnar mesophase (Col_hex) over a wide temperature range. In the film state, associated with the reduction of symmetry from *p6mm* to *p3m1*, the quantum yield of the metallacycle reaches 47.4% at room temperature, much higher than that of previously reported rhomboidal metallacycle-cored liquid crystals and many other luminescent liquid crystals.[33,38] More interestingly, the ionic nanochannels formed by the stacking of these hexagonal metallacycles endow the metallacycles with good ionic

aShaanxi International Research Center for Soft Matter, State Key Laboratory for Mechanical Behavior of Materials, Xi'an Jiaotong University, Xi'an 710049, P. R. China. E-mail: yu.cao@xjtu.edu.cn; mingming.zhang@xjtu.edu.cn

bCollege of Chemistry and Environmental Engineering, Shenzhen University, Shenzhen 518055, P. R. China

cKey Laboratory of Catalytic Materials and Technology of Shaanxi Province, Kaili Catalyst & New Materials Co., Ltd, Xi'an 710201, P. R. China

† Electronic supplementary information (ESI) available. See DOI: https://doi.org/10.1039/d4sc07318e
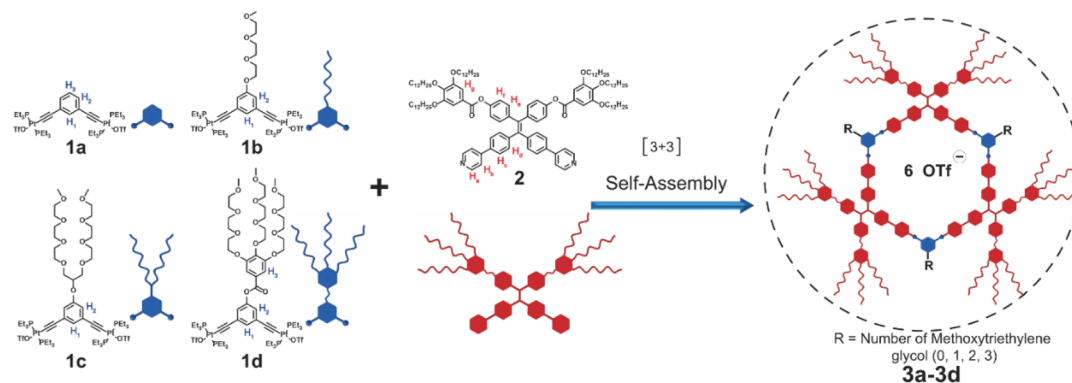
Scheme 1 Cartoon representations of the formation of hexagonal metallacycles **3a–d** *via* metal-coordination-driven self-assembly.

conductivity (1.1×10^{-6} S cm^{-1} at 30 °C) in the liquid crystal-line film at room temperature. This work reveals that hollow hexagonal-shaped metallacycles can form stable mesophases driven by metal coordination and explores a type of luminescent ionic liquid crystals that may be employed as one-dimensional ion-conductive materials in energy-related devices, optoelectronics and sensing.

Results and discussion

Based on the self-assembly of 120° platinum (II) ligands **1a–d** and a dipyridyl tetraphenylethylene (TPE) derivative **2**, hexagonal metallacycles **3a–d** were prepared in good yields (Scheme 1). Metallacycles **3a–d** were characterized by multiple NMR (^{31}P{^{1}H}, ^{1}H, and ^{13}C) analysis and electrospray ionization time-of-flight mass spectrometry (ESI-TOF-MS) (ESI Fig. S1–S60†). All these observations agreed well with previously reported results[33] and suggested the successful preparation of hexagonal metallacycles **3a–d**.

The liquid crystalline properties of metallacycles **3a–d** were investigated by differential scanning calorimetry (DSC), polarized optical microscopy (POM), and small/wide angle X-ray scattering (SAXS/WAXS). Taking **3d** as an example (Fig. 1a), no obvious exothermic/endothermic peaks were observed above room temperature from the DSC curves (Fig. 1b and S61 ESI†). Clear birefringent textures were found for all the metallacycles upon heating (Fig. 1c and S62–S65 ESI†). Due to the same phase type and close melting points of TEG chains and dodecane, the DSC curves and POM textures of **3a–d** were similar to each other. WAXS temperature scans showed obvious diffused peaks at *ca.* 0.45 nm for all the metallacycles (Fig. 1d and S66a–d, ESI†). Particularly, an extra sharp peak at 0.37 nm was seen for **3d** until 130 °C (Fig. 1d), corresponding to the π–π stacking of the adjacent metallacycles, suggesting the increased packing order with the increase of the density of TEG units. All the results suggested the formation of thermotropic liquid crystals above room temperature for all the metallacycles.
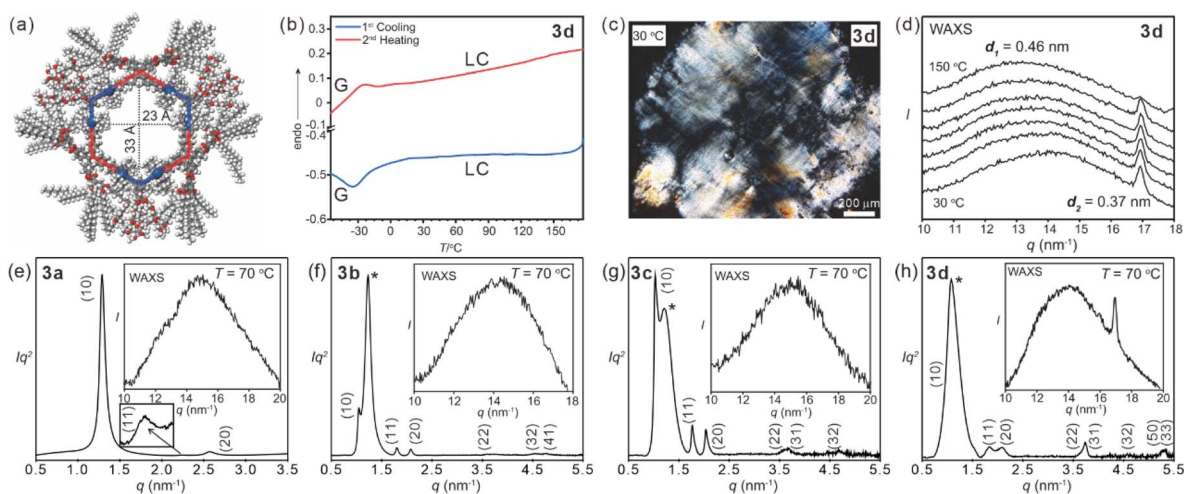

Fig. 1 (a) Molecular model of **3d** optimized by molecular dynamics. The largest hole should be *ca.* 2.3 nm. (b) DSC curves of **3d** upon first cooling and second heating. No obvious exothermic/endothermic peaks can be observed. (c) POM texture after shearing of **3d** at room temperature, exhibiting both birefringence and fluidity. (d) WAXS temperature scan of **3d** from room temperature to 150 °C. The diffused peak d_1 and features from DSC and POM support the liquid crystallinity. Vanishing of d_2 suggests the loss of local order upon heating. (e–h) SAXS/WAXS diffractograms of metallacycles for **3a**, **3b**, **3c** and **3d** at 70 °C. The (10) peak of **3d** is labelled according to the lattice parameter determined by high index peaks.

In order to decipher the liquid crystalline phase, SAXS measurements were performed for metallacycles **3a–d** (Fig. 1e–h, S66e–l and Tables S1–S4 ESI†). For **3a**, the scattering pattern indicated a typical hexagonal lattice with 2D symmetry as the columnar phase (ratio of d-spacings: $1 : 1/3^{1/2} : 1/2$) (Fig. 1e). The lattice parameter a_{hex} of **3a** was 5.61 nm. The reconstructed electron density (ED) map (Fig. 2a) suggested that metallacycle **3a** self-organized into columns (Fig. 2b) owing to the steric effect and nano-segregation caused by the peripheral alkyl chains. From the hollow center (red circular region) to the metallacycles (green region) and then to the peripheral alkyl chains (purple region), the electron density increased gradually, which was consistent with the stacking of **3a** in the columnar phase. Owing to the free-rotating metallacycles and adjacent holes, the spatial and temporal average ED of metallacycles was lower than that of peripheral alkyl chains. Interestingly, for metallacycles **3b–d**, an extra broad peak adjacent to (10) was observed (Fig. 1f–h), indicating the local clusters of TEG units, which indicates the columnar phase of the $p3m1$ plane group (for more details, see Section S7 and Fig. S67†).[33] Correspondingly, the lattice parameter of metallacycles **3b–d** swelled to *ca.* 6.96 nm. The phase separation would inevitably induce the symmetry breaking and reduction of symmetry from hexagonal $p6mm$ for **3a** to trigonal $p3m1$ for **3b–d**. The rarely found $p3m1$ phase was only observed in the bent-core bola-polyphile liquid crystal due to steric effect.[39] Due to its non-centrosymmetric property, the phase combination becomes arbitrary which hinders the reconstruction of the ED map by a simple trial and error. Thus, a theoretical packing model with actual lattice parameters, molecular size and electron density was constructed to estimate the phase angle combination

(Fig. 2c and ESI Section 7†). The Fourier transform of the model, based on positions and shape factor of circular and rectangular components in the proposed model, gives analytical scattering intensities that fit well with experimental results with phase angle combination (Fig. 2d and ESI Table S5†). An alternating ED distribution was seen at the corners of metallacycles **3b–d** based on both experimental and simulated results (Fig. 2e–f and S68 ESI†), suggesting that the rotation of the metallacycles was restricted by the aggregation of peripheral TEG and alkyl chains (Fig. 2g), which would benefit the emission of these metallacycles.

The UV-vis absorption and emission spectra of metallacycles **3a–d** in dichloromethane were collected (Fig. 3a and ESI Fig. S69a–h†). All these metallacycles exhibited three absorption bands centered at *ca.* 266 nm, 299 nm and 357 nm and a broad emission band centered at 510 nm, which was attributed to the TPE units.[33] Upon the gradual addition of hexane into the dichloromethane solution of metallacycles **3a–d**, their emission increased remarkably (Fig. 3b and ESI Fig. S69i–l†), suggesting that the aggregation-induced emission (AIE)[40] feature of TPE was well retained. Thin films of metallacycles **3a–d** were further prepared to study their absorption and emission in the liquid crystalline state at room temperature (Fig. 3c). Three absorption bands centered at 276 nm, 304 and 339 nm were found owing to $n–\sigma^*$, $n–\pi^*$ and $\pi–\pi^*$ transitions, respectively. These metallacycles exhibited a single emission band with the maximum emission centered at 493 nm. The quantum yields (Φ_F) were measured to be 22.8% for **3a**, 18.0% for **3b**, 24.9% for **3c**, and 47.4% for **3d** (Fig. 3d), which were among the highest values of luminescent liquid crystals at room temperature (Fig. S70a†).[38]
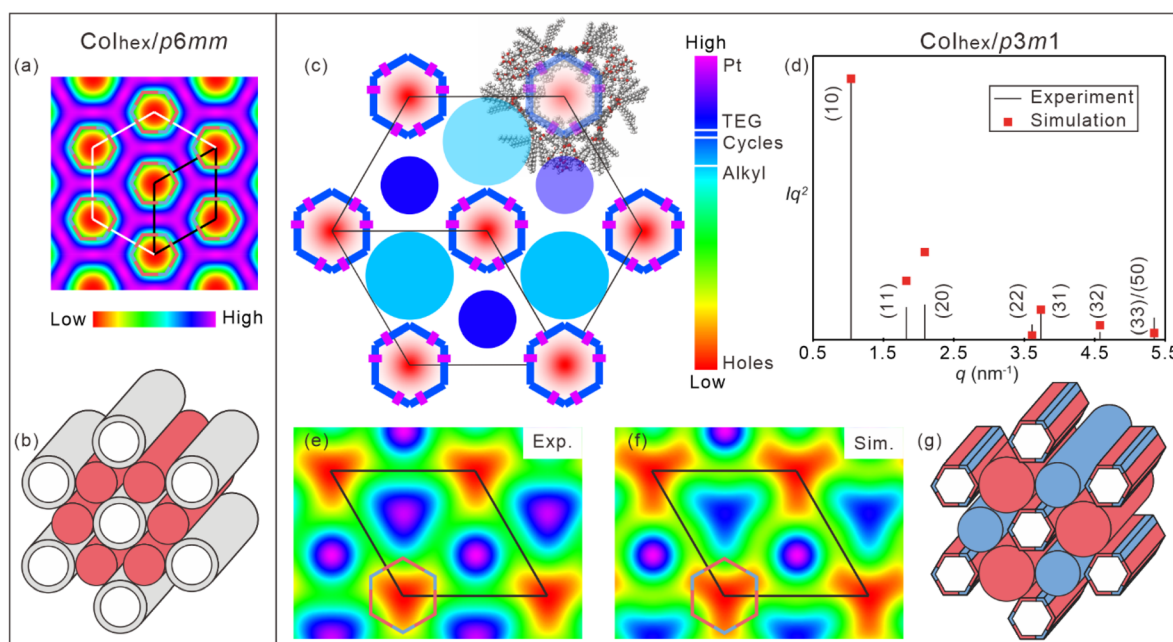
Fig. 2 (a) Reconstructed electron density maps and (b) schematic model of the Col$_{hex}$/$p6mm$ phase. The metallacycles freely rotate to generate the uniform ED in green. (c) Model constructed for the Col$_{hex}$/$p3m1$ phase whose colors are from the normalized electron density. (d) The experimental and simulated SAXS intensities of the indexed peaks. (e and f) Reconstructed electron density maps based on experimental intensities and simulated intensities. The main deviation is from the ED of alkyl chains. (g) Schematic model of the Col$_{hex}$/$p3m1$ phase.
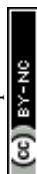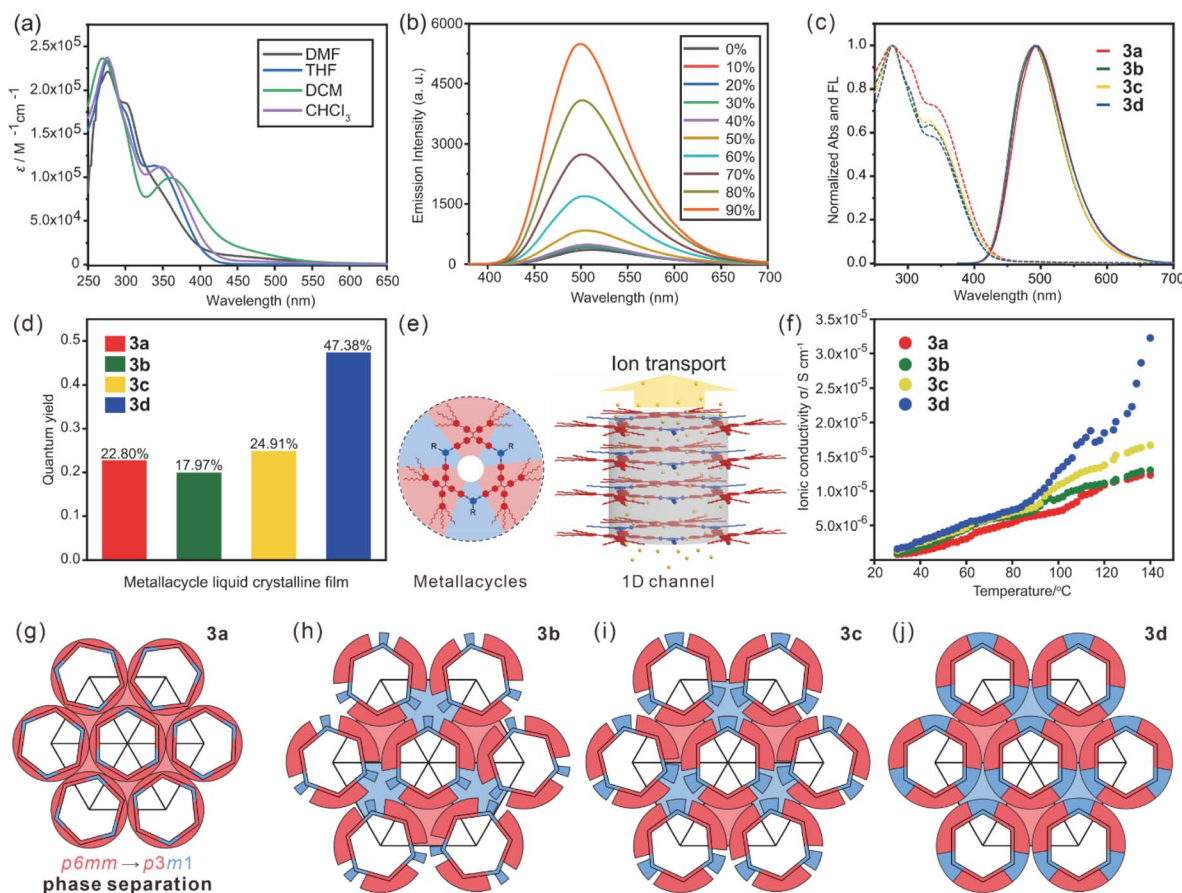
Fig. 3 (a) UV/vis absorption spectra of metallacycles **3d** in different solvents. (b) Emission spectra of **3d** in dichloromethane/hexane (λ_{ex} = 365 nm, c = 10 μM), suggesting the AIE property. (c) Absorption (dashed line), fluorescence emission spectra (solid line) of the liquid crystal film of metallacycles **3a–d**. (d) Quantum yield (Φ_F) of the liquid crystal film of metallacycles **3a–d**. (e) Schematic illustration of the metallacycles and their aggregation with the 1D channel. (f) Ionic conductivities as a function of the temperature of metallacycles **3a–d** in the aligned columnar phases. (g–j) Schematic illustration of the packing of metallacycles **3a–d** in the columnar phases. Introduction of TEG units reduces the hexagonal *p6mm* group (6-fold red shadow) into the trigonal *p3m1* group (3-fold red/blue shadow).

Apart from the luminescence from aggregation, the columnar phase provided intrinsic 1D channels (Fig. 3e). Combining with the positive-charged nature of these metallacycles and the ionic conductivity of TEG units,[41] the ionic conductivities of **3a–d** along the columnar axis were measured by electrochemical impedance spectroscopy. As shown in Fig. 3f, the ionic conductivities of metallacycles **3a–d** increased along with temperature due to the enhanced mobility. At 30 °C, the ionic conductivity was 5.5×10^{-7} S cm^{-1} for **3a**, 6.9×10^{-7} S cm^{-1} for **3b**, 9.4×10^{-7} S cm^{-1} for **3c** and 1.1×10^{-6} S cm^{-1} for **3d**. With the increase of the density of TEG units, the ionic mobility of the metallacycles in the mesophase was enhanced, giving better ionic conductivity comparable with other ionic liquid crystals at room temperature (Fig. S70b†).[42] Integrating with their highly emissive nature and ease of alignment, these metallacycles could be applied in the construction of optoelectrical devices such as LCDs.

Both liquid crystalline phase and properties of these metallacycles were closely related to the phase separation and symmetry breaking. As indicated by ED maps (Fig. 2a and e), metallacycles **3a–d** were packed in the columnar phase with a central hollow of *ca.* 2.1 nm, close to their geometrically optimized molecular model (Fig. 1a). Such a similarity suggested a minor local shift in the crystallographic plane, generating well-organized channels along the columnar axis capable of transporting ions. In order to evaluate the influence of the in-plane steric effect, molecular packing models based on the actual molecular shape and peripheral chain distribution were proposed (Fig. 3g–j). Alkyl chains in red uniformly filled the space between columns of **3a**, providing liquid crystallinity and conventional *p6mm* group.[43] Alkyl chains of **3b–d** were rearranged with blue TPE units as intervals due to phase separation, forming the *p3m1* phase. Obviously, the volume of TPE units was essential for the metallacycle packing. Theoretically, 54.1% volume ratio between TEG and alkyl chains (ESI Fig. S71†) was needed to properly fill the space between neighboring columns. The volume ratio was 11.9% for **3b**, leading to an inevitable local rotation and the lowest Φ_F of 17.8%. Increasing the volume of TEG units gradually restricted the rotation of the metallacycles and thus enhanced the emission of metallacycles **3b–d**. **3d** provided a more desirable volume ratio as large as 42.6%, giving a strong phase separation and good space filling to

regulate the stacking of metallacycles and eventually boost the Φ_F to 47.4%.

Conclusions

In summary, we have successfully constructed a series of hexagonal metallacycles that formed a thermotropic hexagonal columnar mesophase at room temperature. The phase separation inside these liquid crystals further restricts the molecular motion of these metallacycles, providing them with good emission in the film state. Moreover, the ordered packing of these metallacycles in the mesophase offers an organized one-dimensional channel, giving them good ionic conductivity. This study provides a simple yet effective strategy for the construction of highly emissive and ionic conductive liquid crystals via metal-coordination-driven self-assembly, which will open a new avenue for advanced supramolecular materials towards optoelectrical applications.[44,45]

Experimental methods

All reagents and deuterated solvents were purchased as analytical grade and used without further purification. Column chromatography was performed using 300–400 mesh silica gel. Nuclear magnetic resonance spectra were recorded with a Bruker Avance 400 MHz or 600 MHz spectrometer. ^{1}H and ^{13}C NMR chemical shifts are reported relative to residual solvent signals, and ^{31}P{^{1}H} NMR chemical shifts are referenced to an external unlocked sample of 85% H_3PO_4 (δ 0.0). Mass spectra were recorded on a Micromass Quattro II triple-quadrupole mass spectrometer using electrospray ionization with a MassLynx operating system. The UV-vis experiments were conducted on a Lambda 950 absorption spectrophotometer. The fluorescence experiments were conducted on a Hitachi F-7000 fluorescence spectrophotometer. Phase textures of all compounds were fully characterized by polarizing optical microscopy (Olympus BX51-P) in conjunction with a heating stage (Linkam LTS420E) and controller (T95-HS). Optical investigations were carried out under equilibrium conditions between two glass slides that were used without further treatment. Transition enthalpies were determined as obtained from differential scanning calorimetry (DSC) which were recorded on a TA DSC250 (heating and cooling rate: 10 K min^{-1}, peak temperatures). SAXS was conducted in a BL16B1 of SSRF and processed using Nika and Irena macros from the Igor platform.

Data availability

The data supporting this article have been included as part of the ESI.†

Author contributions

L. C.: data curation, investigation, validation, writing – original draft. Y. C.: formal analysis, funding acquisition, investigation, methodology, visualization, writing – review & editing. H. H.: investigation, writing – review & editing. S. L.: investigation,

writing – review & editing. Y. H.: investigation, writing – review & editing. T. T.: investigation, writing – review & editing. X. L.: project administration, writing – review & editing. F. L.: project administration, supervision, writing – review & editing. M. Z.: conceptualization, funding acquisition, project administration, resources, supervision, writing – review & editing.

Conflicts of interest

There are no conflicts to declare.

Acknowledgements

References

1 Z. Liu, S. K. M. Nalluri and J. F. Stoddart, *Chem. Soc. Rev.*, 2017, **46**, 2459–2478.

2 D. Prochowicz, A. Kornowicz and J. Lewiński, *Chem. Rev.*, 2017, **117**, 13461–13501.

3 R. Kumar, A. Sharma, H. Singh, P. Suating, H. S. Kim, K. Sunwoo, I. Shim, B. C. Gibb and J. S. Kim, *Chem. Rev.*, 2019, **119**, 9657–9721.

4 S. J. Barrow, S. Kasera, M. J. Rowland, J. Del Barrio and O. A. Scherman, *Chem. Rev.*, 2015, **115**, 12320–12406.

5 T. Ogoshi, T. Yamagishi and Y. Nakamoto, *Chem. Rev.*, 2016, **116**, 7937–8002.

6 Q. Wang, Y. Zhong, D. P. Miller, X. Lu, Q. Tang, Z. L. Lu, E. Zurek, R. Liu and B. Gong, *J. Am. Chem. Soc.*, 2020, **142**, 2915–2924.

7 M. Stepien, B. Donnio and J. L. Sessler, *Angew. Chem., Int. Ed.*, 2007, **46**, 1431–1435.

8 Y. Luo, N. Marets and T. Kato, *Chem. Sci.*, 2018, **9**, 608–616.

9 M. Fritzsche, A. Bohle, D. Dudenko, U. Baumeister, D. Sebastiani, G. Richardt, H. W. Spiess, M. R. Hansen and S. Hoger, *Angew. Chem., Int. Ed.*, 2011, **50**, 3030–3089.

10 M. Amorin, A. Perez, J. Barbera, H. L. Ozores, J. L. Serrano, J. R. Granja and T. Sierra, *Chem. Commun.*, 2014, **50**, 688–690.

11 K. Guy, P. Ehni, S. Paofai, R. Forschner, C. Roiland, M. Amela-Cortes, S. Cordier, S. Laschat and Y. Molard, *Angew. Chem., Int. Ed.*, 2018, **57**, 11692–11696.

12 P. L. Champagne, D. Ester, D. Polan, V. E. Williams, V. Thangadurai and C. C. Ling, *J. Am. Chem. Soc.*, 2019, **141**, 9217–9224.

13 Y. X. Hu, X. Hao, L. Xu, X. Xie, B. Xiong, Z. Hu, H. Sun, G. Q. Yin, X. Li, H. Peng and H. B. Yang, *J. Am. Chem. Soc.*, 2020, **142**, 6285–6294.

14 Y. X. Hu, X. Hao, D. Wang, Z. C. Zhang, H. Sun, X. D. Xu, X. Xie, X. Shi, H. Peng, H. B. Yang and L. Xu, *Angew. Chem., Int. Ed.*, 2024, **63**, e202315061.

15 T. Kato, J. Uchida, T. Ichikawa and T. Sakamoto, *Angew. Chem., Int. Ed.*, 2018, **57**, 4355–4371.

16 Z. Yu, X. M. Chen, Z. Y. Liu, M. Wang, S. Huang and H. Yang, *Chem. Commun.*, 2021, **57**, 911–914.

17 K. Sato, Y. Itoh and T. Aida, *J. Am. Chem. Soc.*, 2011, **133**, 13767–13769.

18 S. Kawano, Y. Ishida and K. Tanaka, *J. Am. Chem. Soc.*, 2015, **137**, 2295–2302.

19 Y. Li, H. Su, X. Feng, K. Yue, Z. Wang, Z. Lin, X. Zhu, Q. Fu, Z. Zhang, S. Z. D. Cheng and W. B. Zhang, *Polym. Chem.*, 2015, **6**, 827–837.

20 W. Zhang and J. S. Moore, *Angew. Chem., Int. Ed.*, 2006, **45**, 4416–4439.

21 H. Y. Lin, Y. T. Wang, X. Shi, H. B. Yang and L. Xu, *Chem. Soc. Rev.*, 2023, **52**, 1129–1154.

22 Z. Zhang, Z. Zhao, Y. Hou, H. Wang, X. Li, G. He and M. Zhang, *Angew. Chem., Int. Ed.*, 2019, **58**, 8862–8866.

23 Z. Zhang, Z. Zhao, L. Wu, S. Lu, S. Ling, G. Li, L. Xu, L. Ma, Y. Hou, X. Wang, X. Li, G. He, K. Wang, B. Zou and M. Zhang, *J. Am. Chem. Soc.*, 2020, **142**, 2592–2600.

24 Y. Hou, Z. Zhang, S. Lu, J. Yuan, Q. Zhu, W. P. Chen, S. Ling, X. Li, Y.-Z. Zheng, K. Zhu and M. Zhang, *J. Am. Chem. Soc.*, 2020, **142**, 18763–18768.

25 C. Mu, Z. Zhang, Y. Hou, H. Liu, L. Ma, X. Li, S. Ling, G. He and M. Zhang, *Angew. Chem., Int. Ed.*, 2021, **133**, 12401–12405.

26 Y. Hou, Z. Zhang, L. Ma, R. Shi, S. Ling, X. Li, G. He and M. Zhang, *CCS Chem.*, 2022, **4**, 2604–2611.

27 C. Mu, L. Zhang, G. Li, Y. Hou, H. Liu, Z. Zhang, R. Zhang, T. Gao, Y. Qian, C. Guo, G. He and M. Zhang, *Angew. Chem., Int. Ed.*, 2023, **135**, e202311137.

28 K. Gao, Y. Cheng, Z. Zhang, X. Huo, C. Guo, W. Fu, J. Xu, G. L. Hou, X. Shang and M. Zhang, *Angew. Chem., Int. Ed.*, 2024, **136**, e202319488.

29 B. H. Northrop, Y. R. Zheng, C. Ki-Whan and P. J. Stang, *Acc. Chem. Res.*, 2009, **42**, 1554–1563.

30 T. R. Cook, Y.-R. Zheng and P. J. Stang, *Chem. Rev.*, 2013, **113**, 734–777.

31 T. R. Cook and P. J. Stang, *Chem. Rev.*, 2015, **115**, 7001–7045.

32 Z. L. Gong, Z. Q. Li and Y. W. Zhong, *Aggregate*, 2022, **3**, e177.

33 L. Chen, C. Chen, Y. Sun, S. Lu, H. Huo, T. Tan, A. Li, X. Li, G. Ungar, F. Liu and M. Zhang, *Angew. Chem., Int. Ed.*, 2020, **132**, 10143–10150.

34 Y. F. Wang, J. W. Shi, J. H. Chen, W. G. Zhu and E. Baranoff, *J. Mater. Chem. C*, 2015, **3**, 7993–8005.

35 D. Zhao, H. He, X. Gu, L. Guo, K. S. Wong, J. W. Y. Lam and B. Z. Tang, *Adv. Opt. Mater.*, 2016, **4**, 534–539.

36 J. Han, S. Guo, H. Lu, S. Liu, Q. Zhao and W. Huang, *Adv. Opt. Mater.*, 2018, **6**, 1800538.

37 Y. Wu, L. H. You, Z.-Q. Yu, J.-H. Wang, Z. Meng, Y. Liu, X.-S. Li, K. Fu, X.-K. Ren and B. Z. Tang, *ACS Mater. Lett.*, 2020, **2**, 505–510.

38 C. Cuerva, M. Cane and C. Lodeiro, *Chem. Rev.*, 2021, **121**, 12107–13010.

39 B. Glettner, F. Liu, X. B. Zeng, M. Prehm, U. Baumeister, G. Ungar and C. Tschierske, *Angew. Chem., Int. Ed.*, 2008, **47**, 6080–6083.

40 J. Mei, N. L. C. Leung, R. T. K. Kwok, J. W. Y. Lam and B. Z. Tang, *Chem. Rev.*, 2015, **115**, 11718–11940.

41 Z. Su, J. Huang, W. Shan, X. Y. Yan, R. Zhang, T. Liu, Y. Liu, Q. Y. Guo, F. Bian, X. Miao, M. Huang and S. Z. D. Cheng, *CCS Chem.*, 2021, **3**, 1434–1444.

42 S. Dou, S. Zhang, R. J. Klein, J. Runt and R. H. Colby, *Chem. Mater.*, 2006, **18**, 4288–4295.

43 K. Goossens, K. Lava, C. R. Bielawski and K. Binnemans, *Chem. Rev.*, 2016, **116**, 4643–4807.

44 B. Soberats, M. Yoshio, T. Ichikawa, H. Ohno and T. Kato, *J. Mater. Chem. A*, 2015, **3**, 11232–11238.

45 B. Soberats, M. Yoshio, T. Ichikawa, X. B. Zeng, H. Ohno, G. Ungar and T. Kato, *J. Am. Chem. Soc.*, 2015, **137**, 13212–13215.